EDGE ARTICLE

Check for updates

Tuning the photocaged spiropyran photoswitch with a sterically hindered adamantane group: releasing the stable merocyanine

Yifan Su,[†a] Xiang Li,[†b] Dexin Zheng,[†a] Joakim Andreásson, [c] Hong Wang,[b] Le Yu,*[d] Jian Chen,*[b] Jiani Ma [*a] and Yu Fang [a]

Molecular photoswitches isomerize between two or more forms by exposure to light or by thermal processes, accompanied by color changes. Spiropyran (SP) derivatives are widely studied. The stable colorless SP form photoisomerizes to the colored merocyanine (MC) form by UV exposure, whereas the reverse reaction is triggered by visible light or in a thermal reaction. Based on our previously reported (*J. Am. Chem. Soc.*, 2018, **140**, 14069) photolabile *o*-nitrobenzyl caged merocyanine switch (denoted as **in-MC**) and a negative photochromic spiro[azahomoadamantane-pyran] (*Anal. Bioanal. Chem.*, 2023, **415**, 715), we have designed a novel multiphotochromic molecule, **ad-MC**, by combining an adamantane-containing negative photochromic unit (**2MC**) and *o*-nitrobenzyl. A wavelength dependent photorelease of the stable **2MC** form is demonstrated for the first time. The detailed photochemical reaction mechanisms of **ad-MC** and **in-MC** were investigated using femtosecond transient absorption spectroscopy and DFT/TD-DFT calculations. The results show that the photochemical mechanisms are the same for both molecules, but the variation in excited state hydrogen transfer barriers' heights leads to the observed differences in photolysis yields and rates of decaging. The structure–reactivity relationships revealed for **ad-MC** and **in-MC** expand the diversity and functionality of SP-based photoswitches for promising utilization in chemical biology applications.

1 Introduction

Photochromism implies reversible color changes induced by exposure to light. Compounds possessing this property are referred to photochromic molecules, or molecular photoswitches. Typical isomerization modes are *E*/*Z* interconversions and ring-closing/opening reactions.[1–8] Popular examples of the latter mode are spiropyrans (SP), where the isomerization reactions imply both geometric and electronic modifications in the molecular structure.[9] The geometric changes can be harnessed for applications in photonic devices, while the electronic changes enable the development of optical memory systems and photoswitching materials.[10–15] SP have emerged as one of the most versatile molecular switches due to their remarkable responsiveness to multiple external stimuli, including pH, solvent polarity, and the wavelength used to trigger the photo-isomerization reactions.[16] Irradiation of the SP isomer with UV-light induces heterolytic cleavage of the strained C_{spiro}–O bond, generating a planar, highly conjugated merocyanine (MC) isomer. More importantly, this photoisomerization is reversible as the MC isomer undergoes ring closure and reverts to SP in response to visible light irradiation (at ~550 nm) or heat.[17]

The use of photolabile protecting groups (PPGs), also known as photocages, is another approach to introduce photo-functionality to molecules in diverse fields of research and practical applications. Examples of such chemical tools include photocaged proteins, nucleotides, ions, neurotransmitters, pharmaceuticals, fluorescent dyes, and small molecules.[18–24] The "masking" of the chemical or biological activity of these compounds is achieved through covalent attachment to a PPG platform. Upon irradiation at a specific wavelength, the PPG moiety is cleaved off, enabling spatiotemporal control of molecular release with high chemo-selectivity in a non-invasive manner. *o*-Nitrobenzyl derivatives are among the most widely used PPGs due to their exceptional photolysis efficiency, straightforward synthesis, excellent solubility, and versatile chemical functionalization pathways.[25,26]

[a]Key Laboratory of Applied Surface and Colloid Chemistry of Ministry of Education, Shaanxi Provincial Key Laboratory of New Concept Sensors and Molecular Materials, School of Chemistry and Chemical Engineering, Shaanxi Normal University, Xi'an 710119, China. E-mail: majiani@snnu.edu.cn

[b]Key Laboratory of Theoretical Organic Chemistry and Functional Molecule of Ministry of Education, School of Chemistry and Chemical Engineering, Hunan University of Science and Technology, Xiangtan, Hunan 411201, China. E-mail: cj920@foxmail.com

[c]Department of Chemistry and Chemical Engineering, Chemistry and Biochemistry, Chalmers University of Technology, SE-41296 Göteborg, Sweden

[d]Key Laboratory of Synthetic and Natural Functional Molecule Chemistry of Ministry of Education, College of Chemistry and Materials Science, Northwest University, Xi'an 710127, China. E-mail: yule@nwu.edu.cn

† Joint first authors.

There has been a growing demand to develop multi-photofunctional molecular systems,[27] such as those combining both photoisomerization and photodecaging, which provides additional advantages and functionalities.[28–36] Previously, we reported a multi-photofunctional molecule—a photocaged switch (denoted as **in-MC**) by linking the MC group to an *o*-nitrobenzyl unit (Scheme 1a).[37] After the photodecaging, the corresponding MC (denoted as **1MC**) is released. The MC form is isomerized to the SP form (denoted as **1SP**) by visible light irradiation or in a thermal reaction. Recently, we developed a novel negative photochromic system by transforming the cyanine part of the traditional SP into a large rigid azahomoadamantane group, which exhibits a stable fluorescent MC form (denoted as **2MC**). **2MC** can be switched to the unstable **2SP** state under visible light irradiation, whereas the thermally unstable SP form (denoted as **2SP**) is non-fluorescent, and spontaneously reverts to the fluorescent **2MC** form in the dark (Scheme 1b).[38] Apparently, low-energy visible photons can reduce the photobleaching damage to the molecules, as high energy UV-light can be avoided, thus endowing this compound with better photostability and photo-reversibility.

With the purpose of releasing the stable fluorescent MC form for potential use in biological imaging, and to obtain a photoswitch with improved photostability and photo-reversibility, we here strategically integrated the adamantane-containing negative photochromic unit (**2MC**) and an *o*-nitrobenzyl PPG, successfully synthesizing the target molecule **ad-MC** (Scheme 1c). The photophysical properties of **ad-MC** were investigated and unravelled the efficient photorelease of **2MC**. Femtosecond transient absorption (fs-TA) spectroscopy was employed to monitor the temporal evolution of reaction intermediates throughout the photochemical processes. Time-dependent and density functional theory (TD-DFT and DFT) calculations were conducted to validate the experimental spectral assignments and to provide mechanistic insights into the reaction pathways. To gain a deeper understanding of the relationship between the chemical structures and photochemical behaviors, the photochemical reaction mechanism of **in-MC** was also investigated and compared with that of **ad-MC**. Details of the results and discussion are elaborated below.

2 Results and discussion

2.1 Photophysical and photochemical properties of ad-MC and comparison with in-MC

The UV-vis absorption spectrum of **ad-MC** in ethanol (EtOH) demonstrates two distinct absorption bands at 300 nm and 360 nm (Fig. 1a), which are assigned to the *trans* configuration (denoted as ***trans*-ad-MC**). The assignment is supported by the TD-DFT simulated electronic absorption spectrum (Fig. 1b). We simulated the spectra of ***trans*-ad-MC** at selected theoretical levels which are commonly used for organic molecules (Fig. S8). We considered that the results obtained from TD-PBE0/def2-TZVP were in sufficiently good agreement with the experimental spectrum of ***trans*-ad-MC**. Thus, the calculations in this work were all performed using this method. Upon irradiation with 300 nm light, the characteristic bands of ***trans*-ad-MC** diminished, while a weak but detectable increase in absorbance was observed around 250 nm (Fig. 1a). In addition, the absorption at 325 nm is only slightly reduced, probably due to the contribution of the generated *cis* configuration (denoted as ***cis*-ad-MC**). These observations suggest that the spectral changes presented in Fig. 1a are due to the *trans* → *cis* isomerization, a conclusion further supported by ^{1}H-NMR analysis (Fig. 1d). The vinylic protons of ***trans*-ad-MC** exhibit a chemical shift at 8.07 ppm, which shifts to 6.85 ppm upon irradiation
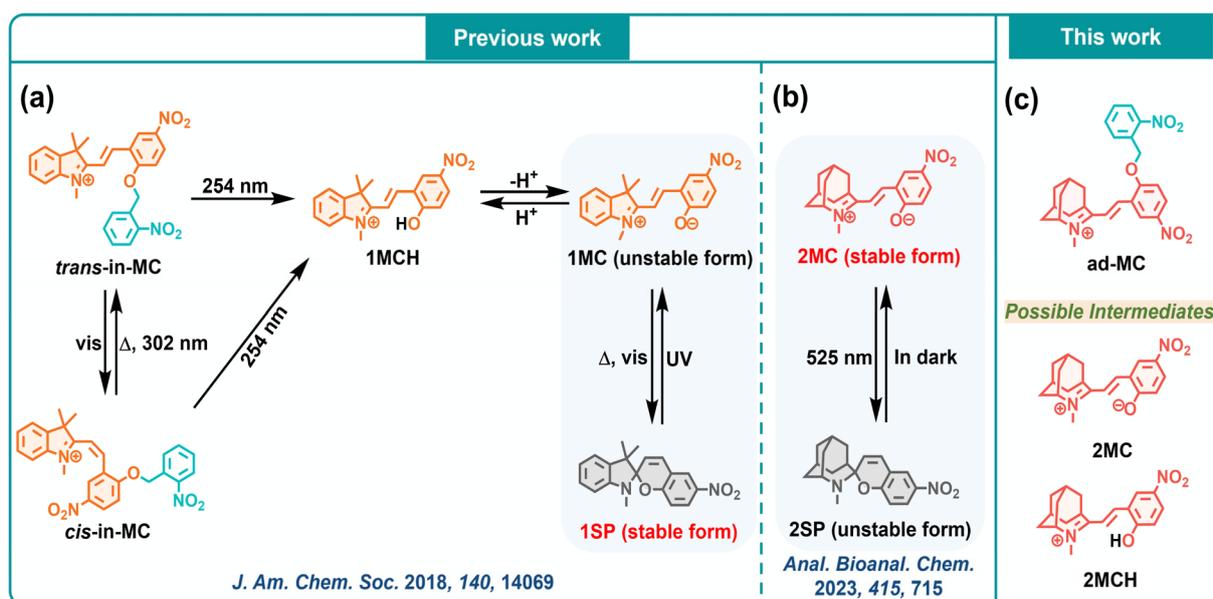
Scheme 1 (a) The photochemical reaction scheme of **in-MC**,[37] (b) the stabilized **2MC** form and the unstabilized **2SP** form,[38] and (c) the molecular structure of **ad-MC** and possible intermediates investigated in this work.
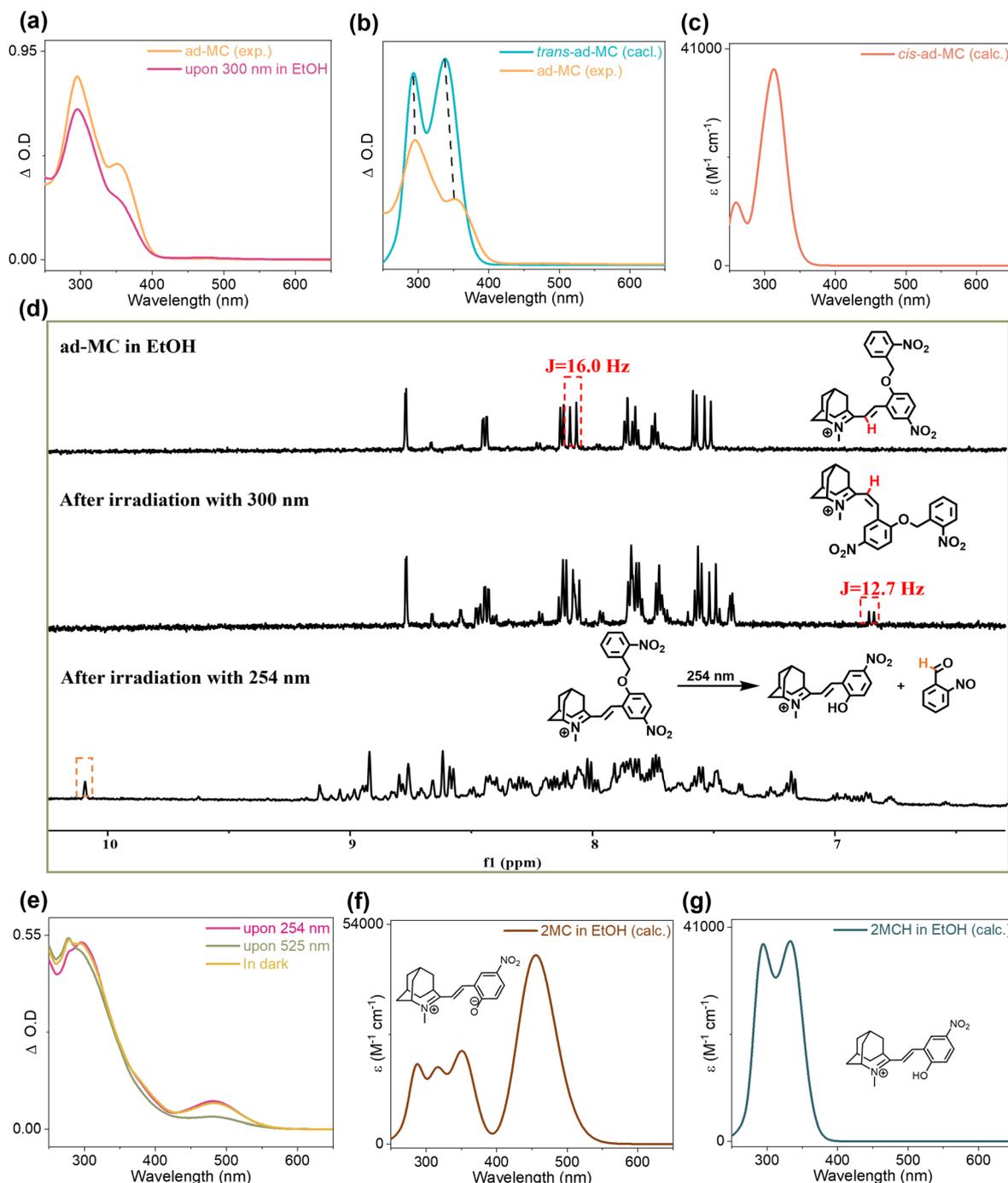
Fig. 1 (a) Steady state absorption spectra of **ad-MC** in EtOH ($\lambda_{ex} = 300$ nm). (b) Comparison of the computed electronic absorption spectrum of **trans-ad-MC** with the UV-vis absorption spectrum of **ad-MC**. (c) The computed electronic absorption spectrum of **cis-ad-MC**. (d) ^{1}H-NMR spectra of **ad-MC** in EtOH-d_6. (e) The absorption spectra of **ad-MC** after irradiation with 254 nm light, subsequent irradiation with visible light (525 nm), and storage in the dark. The simulated electronic absorption spectra of (f) **2MC** and (g) **2MCH** (TD-PBE0/def2-TZVP (EtOH) with a scale factor of 1.00 and a half-width of 1500 cm^{-1}).

with 300 nm light. Moreover, the coupling constant decreases from 16.0 Hz to 12.7 Hz, indicating *trans → cis* isomerization. UV-vis absorption experiments were also conducted in dichloromethane (DCM), where similar spectral changes are observed (Fig. S9a). However, the decrease in absorbance after irradiation is less pronounced compared to the results in EtOH,

and no significant changes are detected in the ^{1}H-NMR spectrum (Fig. S9b). This discrepancy may be attributed to the influence of solvent polarity on the electron distribution and energy levels of the molecules, which in turn affects the activation energy and reaction rate of the isomerization process.[39]

In our previous study, the irradiation with 254 nm light induces the photorelease of the o-nitrobenzyl group from the phenolate oxygen of **in-MC**, leading to the formation of **1MC** through an intermediate **1MCH** (as illustrated in Scheme 1a).[37] The steady-state UV-vis spectrum of **ad-MC** was recorded in EtOH following irradiation with 254 nm light (Fig. 1e). Upon excitation, the absorption signals corresponding to ***trans*-ad-MC** decreased, and a new absorption band emerged at 480 nm. By comparing the experimental results with the simulated electronic absorption spectra of **2MC** and **2MCH** obtained through TD-DFT calculations (Fig. 1f and g), the product observed at 480 nm can be identified as **2MC**. Analysis of the ^{1}H-NMR spectra of **ad-MC** before and after 254 nm irradiation (Fig. 1d) reveals the emergence of a distinct absorption peak at 10.01 ppm. This is assigned to the aldehyde proton signal of o-nitrosobenzaldehyde, which is the photolysis product. These findings confirm the successful photochemical transformation of **ad-MC** upon 254 nm irradiation, yielding the anticipated photorelease product with a photolysis yield of 0.19. When exposing **ad-MC** to 254 nm light in DCM, a new intermediate was observed at 295 and 370 nm and was attributed to **2MCH** (Fig. S9c–e). In addition, a weak band was observed at 510 nm indicating the formation of **2MC**. The red-shift in the **2MC** absorption from 480 nm in EtOH to 510 nm in DCM is consistent with the established negative solvatochromism for the MC form, and is also supported by the simulated electronic absorption spectrum. **2MC** was obviously observed in EtOH, while both **2MC** and **2MCH** were detected in DCM. This is attributed to the caging effect of EtOH, which favors the formation of **2MC**. Additionally, EtOH facilitates proton transfer, leading to higher photorelease efficiency. However, experiments conducted in DCM rule out the influence of the solvent cage effect, thereby allowing the detection of **2MCH**. The photochemical reaction of **ad-MC** is more efficiently observed experimentally in protic solvents, suggesting that improving the water solubility could facilitate its application in aqueous environments.

Upon irradiation with visible light at 525 nm, **2MC** undergoes a transformation into the **2SP** form (Fig. 1e and Scheme 1b). During this process, the absorbance at 480 nm diminishes. The system spontaneously reverts to **2MC** in the dark.
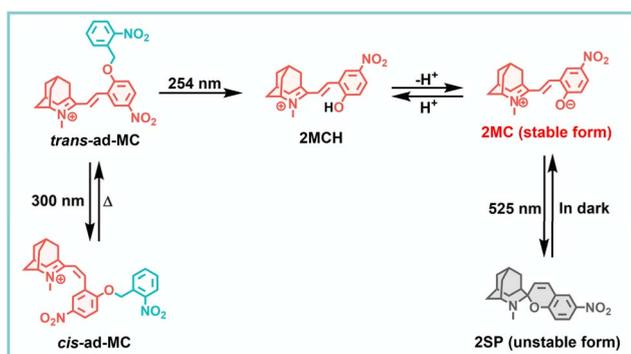
Scheme 2 The photochemical pathways of **ad-MC**.

As summarized in Scheme 2, exposure of **ad-MC** to UV light at 300 nm induces the *trans → cis* isomerization. On the other hand, irradiation at 254 nm initiates photorelease, resulting in the formation of **2MCH**. Subsequent deprotonation of the hydroxyl group in **2MCH** generates the negative photochromic molecule **2MC** (*vide infra*). Finally, upon visible light irradiation (525 nm), **2MC** converts to its ring-closed form (**2SP**), which spontaneously reverts to **2MC** in the dark.

Based on the photochemical reaction studies of **ad-MC**, we found that its behavior differs significantly from that of the previously reported **in-MC**. Previous studies have shown that **2MC** is more stable than **2SP**, while **1SP** is more stable than **1MC**,[37,38] and the same conclusion was reached by theoretical calculations (Tables S2 and S4). Consequently, **ad-MC** and **in-MC** exhibit unique properties that make them suitable for different applications. To elucidate their photochemical reactivity differences, we conducted comparative reaction studies on both molecules (Fig. S10). Under 260 nm irradiation, for **in-MC**, a decrease in absorption at 300 nm and 395 nm and an increase in absorption at 540 nm was observed. Similarly, **ad-MC** exhibited decreased absorption at 300 nm and 360 nm, with a concurrent increase at 480 nm. Interestingly, the photorelease rate constant of **in-MC** was 45.9×10^{-4} s^{-1}, while that of **ad-MC** was 121.8×10^{-4} s^{-1}, clearly showing a faster photorelease process for **ad-MC** compared to **in-MC**. This is also reflected in the photolysis yields for **in-MC** and **ad-MC** determined by ^{1}H-NMR. The photolysis yield of **in-MC** is determined to be 0.12, which is lower than that of **ad-MC** (0.19) (Fig. S11). The superior release kinetics and photolysis yield of **ad-MC** relative to **in-MC** establish it as a more promising PPG candidate.

2.2 Photochemical reaction mechanism studies of ad-MC and in-MC

Ultrafast transient absorption spectroscopy and DFT/TD-DFT calculations were combined to unravel the mechanistic basis for the different properties of **ad-MC** and **in-MC**.

Fig. 2a presents the fs-TA spectra of **ad-MC** in EtOH following 266 nm excitation (the available wavelength closest to 254 nm). Upon excitation, excited state absorptions emerged at 340, 400 and 435 nm. The signal at 340 nm subsequently decayed, while the 400 nm band red-shifted to 420 nm. Simultaneously, a new absorption band appeared at 510 nm, and the signal at 435 nm decayed. Over time, the signals at 420 nm and 510 nm decreased, giving rise to a new species with an absorption peak at 335 nm. The presence of an isosbestic point at 380 nm suggests that the species at 420 nm and 510 nm is the precursor to the one at 335 nm. The fs-TA results in DCM are similar to those observed in EtOH (Fig. S12).

As illustrated in the schematic energy diagram (Fig. 2b), upon irradiation at 266 nm light, ***trans*-ad-MC** is initially pumped to the Franck–Condon region of highly excited states, then rapid internal conversion occurs to yield the singlet excited state (***trans*-ad-MC(S$_1$)**) minimum (73.6 kcal mol^{-1}). Subsequently, ***trans*-ad-MC(S$_1$)** undergoes a hydrogen transfer process by overcoming a reaction energy barrier through 2TS1 to yield an *aci*-nitro form product (2CI) which serves as a conical
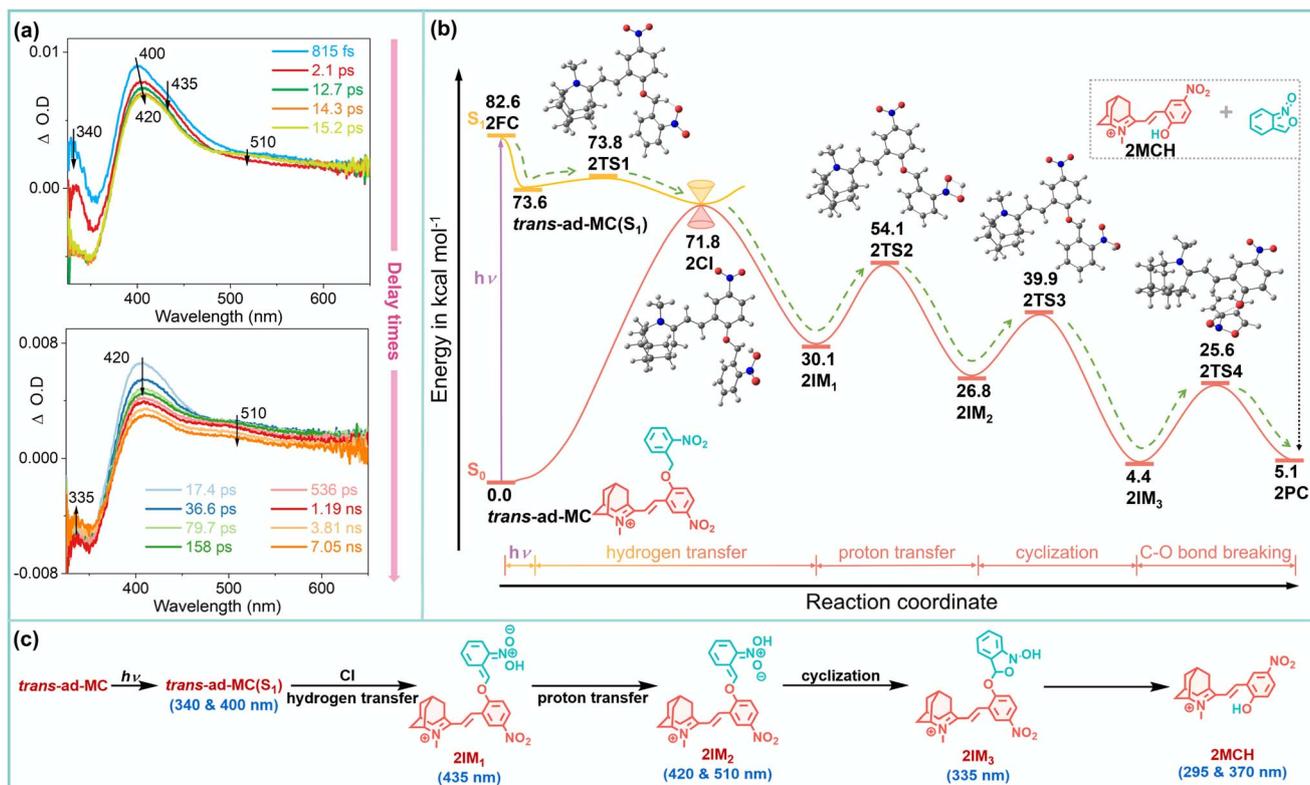
Fig. 2 (a) fs-TA spectra of **ad-MC** in EtOH (λ_{ex} = 266 nm). (b) The PES of the photochemical reaction of **ad-MC** (PBE0/def2-TZVP (EtOH)). (c) Photorelease reaction mechanism of **ad-MC**.

intersection between the S_1 and S_0 states. After internal conversion, the ground-state intermediate $2IM_1$ is generated, then the *aci*-nitro proton migrates to the neighbor oxygen ($2IM_2$, 26.8 kcal mol^{-1}) by overcoming an energy barrier of 24.0 kcal mol^{-1} ($2TS2$). Additionally, the meta-stable $2IM_2$ can undergo a cyclization process to form the stable species $2IM_3$ (4.4 kcal mol^{-1}) *via* $2TS3$ (39.9 kcal mol^{-1}). Finally, $2IM_3$ undergoes a synchronous C–O bond breaking and proton transfer process by overcoming a potential barrier of 21.2 kcal mol^{-1} ($2TS4$), and ultimately rearranges to release **2MCH**. Although the potential energy surface (PES) in Fig. 2 suggests the $2IM_3 \rightarrow 2PC$ process is slightly endothermic, the corresponding Gibbs free energy change is −2.6 kcal mol^{-1} (Table S3), implying a spontaneous deprotection. In addition, the vibrational hot state of 2,1-benzisoxazole, 1-oxide can undergo a barrierless process to generate *o*-nitrosobenzaldehyde (Fig. S13). This agrees with the results of photochemical tests, explaining the experimental detection of the photorelease product of **ad-MC** pumped by 254 nm light.

We then assigned the intermediate species observed in the fs-TA spectra to the corresponding intermediates identified in the PES calculations. Based on a comparison between the characteristic fs-TA spectra and the simulated electronic spectra derived from TD-DFT calculations, we made the following assignments (Fig. S14 and Fig. 2c): the intermediate with absorption signals at 340 and 400 nm can be assigned to *trans*-**ad-MC**(S_1), while the signal at 435 nm was attributed to $2IM_1$.

The fs-TA spectra show that the signal of $2IM_1$ (435 nm) is weaker in EtOH than in DCM. This is rationalized by the fact that EtOH, a protic solvent, facilitates the proton transfer process for the conversion of $2IM_1$ to $2IM_2$. Given that water is also a protic solvent, a similarly rapid reaction rate is anticipated in biological (aqueous) environments. The species exhibiting absorption at 420 and 510 nm was identified as $2IM_2$, while the absorption at 335 nm was assigned to $2IM_3$.

The fs-TA experiments were also conducted on **ad-MC** under 300 nm excitation in both EtOH and DCM (Fig. S15 and S16), and the results were similar to those observed under 266 nm excitation. Specifically, the intermediates *trans*-**ad-MC**(S_1), $2IM_1$, $2IM_2$, and $2IM_3$ were detected (Fig. S17). However, the signal of **2MCH** is absent in the steady state absorption spectra upon 300 nm irradiation, implying the deprotection process is not taking place. This will be discussed in detail later.

To understand the structure–property relationship, reaction mechanism studies were further conducted for the previously studied multi-functional photoswitch **in-MC**. fs-TA spectra of **in-MC** were recorded in EtOH (Fig. S19) and the signals were attributed to *trans*-**in-MC**(S_1), $1IM_1$, $1IM_2$ and $1IM_3$, in conjunction with theoretical calculations (Fig. S20).

The PES for the photorelease process of **in-MC** is shown in Fig. 3, which is generally similar to **ad-MC** in its photorelease process. *trans*-**in-MC** is initially excited to the high-lying excited state, and after rapidly relaxes to the first singlet excited state (*trans*-**in-MC**(S_1)), which then transforms to 1CI for non-
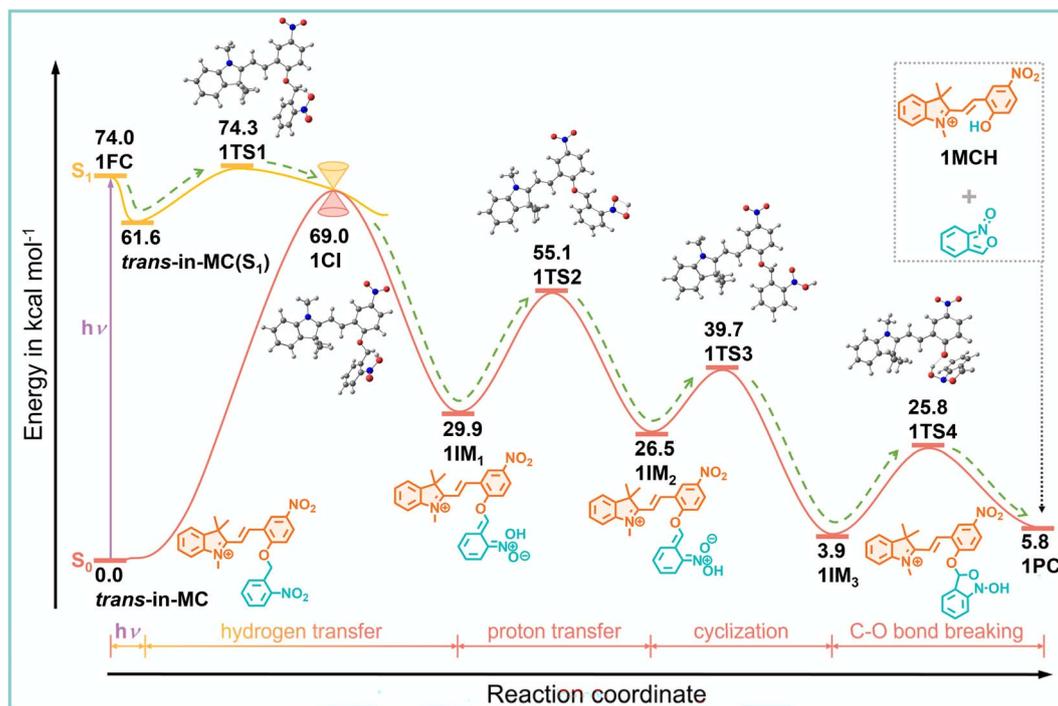
Fig. 3 The PES of the photochemical reaction of **in-MC** (PBE0/def2-TZVP (EtOH)).

adiabatic decay to the S_0 state. Subsequently, **in-MC** undergoes hydrogen transfer, proton transfer and cyclization coupled C–O bond dissociation processes sequentially *via* intermediates $1IM_1$, $1IM_2$, and $1IM_3$, respectively, which ultimately leads to the release of **1MCH**.

As illustrated in Fig. 2 and 3, the photorelease mechanisms of **in-MC** and **ad-MC** are generally the same, and both exhibit excitation wavelength selectivity due to stepwise processes *via* different reaction coordinates. Furthermore, the energetically favored *trans → cis* isomerization (Fig. S21) competes with the deprotection of **ad-MC** and **in-MC**, and overall limits the branching ratio of MC releasing.

On the other hand, it is noted that both the photolysis yield and rate constant of the photorelease process for **ad-MC** have been greatly improved with respect to **in-MC**. This fact can be traced back to the stability of the *trans* form in the S_1 state. The relative energy of ***trans*-in-MC(S_1)** is 12.0 kcal mol^{-1} lower than ***trans*-ad-MC(S_1)** due to the extended conjugation system, and the corresponding barrier height for hydrogen transfer (*trans → cis* isomerization) are 12.7 (3.7) kcal mol^{-1} and 0.2 (3.3) kcal mol^{-1}, respectively. Obviously, the reduced hydrogen transfer barrier for ***trans*-ad-MC(S_1)** not only significantly increases the photorelease rate, since it serves as the precursor to the subsequent steps to complete the overall photoreleasing reaction, but also makes the photorelease reaction more competitive compared to the *trans → cis* isomerization pathway.

It is not surprising that the photorelease yields of **ad-MC** and **in-MC** are relatively low since various steps corresponding to different reaction modes need to be accomplished prior to

deprotection. To improve the photorelease efficiency of MC-based systems, the following could be considered: first, more nitro groups could be introduced to the *o*-nitrobenzyl group to enhance the acidity of the benzyl hydrogen, and thus promote the branching ratio of the deprotection reaction. Moreover, the reduced S_1 state hydrogen transfer barrier would imply that the photorelease can be activated with lower irradiation energy. Second, enhancing the rigidity of the MC backbone or introducing steric hindrance to restrict the –C=C– twisting would be beneficial. Although the MC derivative may lose the multi-photochromic character, the deprotection capability would be improved.

Notably, both **in-MC** and **ad-MC** utilize *o*-nitrobenzyl groups enabling UV-light-triggered release. To broaden the photo-pharmacological applicability, the *o*-nitrobenzyl group could be replaced by PPGs absorbing above 600 nm,[40] a spectral region where neither MC nor MCH exhibits absorption.

2.3 Why no photorelease reaction occurs for ad-MC and in-MC at longer excitation wavelengths

The fs-TA studies on **ad-MC** under excitation by both 266 nm and 300 nm probed the same processes of hydrogen transfer, proton transfer and cyclization. On the other hand, the steady-state spectroscopic analysis revealed that only the short wavelength can trigger the photorelease reaction for the two molecules. That suggests that the key is the C–O bond dissociation, which is the last step during the photorelease process as indicated by DFT calculations. It is thus interesting to unravel how the wavelength decides the different photochemical behaviours of **ad-MC** and **in-MC**.

Upon photoexcitation, the absorbed photon energy disperses into potential energy that determines which electronic state the system is in and kinetic energy that drives the molecule's evolution. Within the following non-radiative relaxation process, the potential energy spontaneously converts to kinetic energy *via* the vibration modes coupled with the reaction coordinates and then dissipates to surrounding solvent. For the multi-step reaction process, if the two consecutive steps follow similar reaction coordinates, this can be achieved easily with the highly efficient vibration energy redistribution. On the other hand, switching to divergent reaction coordinates after the first step is unfeasible compared to dissipating to the surroundings.

For **ad-MC**, the reaction coordinate switching takes place after hydrogen transfer, proton transfer and cyclization along the photoinduced deprotection reaction pathway, overcoming energy barriers of 0.2, 24.0 and 13.1 kcal mol^{-1}, respectively. However, the first three reaction processes are thermodynamically favored exothermic reactions, where the reactant could spontaneously convert to product to achieve a more stable condition despite being hindered by a substantial barrier. When the molecule transforms to **2IM$_3$**, it is only 4.4 kcal mol^{-1} higher than *trans*-**ad-MC**(S$_0$), and thus can be considered as an intermediate product with the initial potential energy being entirely consumed. Therefore, the following deprotection with a conserved energy change *via* a 21.2 kcal mol^{-1} barrier becomes the controlling step of the multi-step wavelength dependent release process. To facilitate the deprotection reaction employing synergetic C–O dissociation and hydrogen transfer modes, a complex vibration redistribution is required and thus a large amount of kinetic energy is stored in modes that are independent of the reaction coordinates of the previous reaction steps as this is better for the reaction efficiency of the current step. Consequently, for the photochemical reaction of **ad-MC**, the initial kinetic energy (equal to the difference between the 300 or 266/254 nm photon and the S$_0 \rightarrow$ S$_1$ vertical excitation energy of *trans*-**ad-MC**) absorbed from the photon will be responsible for overcoming the 2TS4 barrier. Upon 300 nm excitation in EtOH, the excess kinetic energy for **ad-MC** is 12.7 kcal mol^{-1}. Compared to the deprotection barrier of 21.2 kcal mol^{-1} for **ad-MC**, the 300 nm photon is insufficient to trigger the C–O bond breaking reaction and the photochemical process is trapped after the cyclization process (Table S7). On the other hand, the excess kinetic energy after 266/254 nm excitation for **ad-MC** is 24.9/30.0 kcal mol^{-1}, which guarantees the C–O bond breaking step and finally forms the released product. The same conclusion is found in DCM. An analogous process applies to **in-MC**. For **in-MC**, photodeprotection occurs upon 254/266 nm irradiation, while *cis–trans* isomerization takes place under 405 nm light. The theoretical calculations show that the excess kinetic energy available at 254/266 nm excitation is also sufficient to overcome the energy barrier for the C–O bond breaking process (Table S8).

3   Conclusions

In conclusion, we have designed a spiropyran-based photoswitch by connecting the *o*-nitrobenzyl photocage with the adamantane-containing negative photochromic unit. Upon irradiation, a stable fluorescent MC form is released which can be photoisomerized to the unstable SP state under visible light irradiation, shining new light on the utilization of this multifunctional photoswitch in chemical biology applications. The photorelease reactions for **ad-MC** and **in-MC** undergo a similar photochemical reaction mechanism of sequential hydrogen transfer, proton transfer, cyclization, and C–O bond breaking processes. On the other hand, **ad-MC** achieves a higher photolysis yield than **in-MC** due to the nearly barrierless transition from the S$_1$ state to the conical intersection. Moreover, it increases the photorelease rate constant of **ad-MC**. Furthermore, product analysis of **ad-MC** and **in-MC** unravels that the photorelease is triggered by 266/254 nm irradiation, while 300 nm excitation has no effect on the decaging. To sum up, the first step during the overall photorelease process decides the photorelease yield and rate for both **ad-MC** and **in-MC**, while the last step determines the wavelength-dependent behavior.

Building on in-depth investigations of reaction mechanisms, this study unveils the structure–reactivity relationship of the multifunctional molecule, offering critical insights for the utilization of such molecules in chemical biology applications.

Author contributions

Yifan Su, Xiang Li and Dexin Zheng: investigation, methodology, data curation, visualization, software and writing – original draft. Joakim Andreásson: investigation, methodology and writing – review & editing. Hong Wang and Jian Chen: investigation, supervision and writing – review & editing. Le Yu: theoretical calculations, supervision and writing – review & editing. Jiani Ma: resources, validation, investigation, data curation, supervision and writing – review & editing. Yu Fang: investigation, supervision and writing – review & editing.

Conflicts of interest

There are no conflicts to declare.

Data availability

The data that support the findings of this study are available in the supplementary information (SI). Supplementary information: synthesis and characterisation (Fig. S1–S7), experimental results and their comparison with computational results (Fig. S8–S21), computational data (Tables S1–S8), and molecular coordinates from theoretical calculations (Table S9).[37,38,41] See DOI: **https://doi.org/10.1039/d5sc06627a**.

Acknowledgements

References

1 J. Harada, M. Taira and K. Ogawa, *Cryst. Growth Des.*, 2017, **17**, 2682–2687.

2 M. A. Kochman, T. Gryber, B. Durbeej and A. Kubas, *Phys. Chem. Chem. Phys.*, 2022, **24**, 18103–18118.

3 P. Kobauri, F. J. Dekker, W. Szymanski and B. L. Feringa, *Angew. Chem., Int. Ed.*, 2023, **62**, e202300681.

4 J. Volarić, W. Szymanski, N. A. Simeth and B. L. Feringa, *Chem. Soc. Rev.*, 2021, **50**, 12377–12449.

5 A. B. Grommet, L. M. Lee and R. Klajn, *Acc. Chem. Res.*, 2020, **53**, 2600–2610.

6 M. M. Lerch, M. J. Hansen, W. A. Velema, W. Szymanski and B. L. Feringa, *Nat. Commun.*, 2016, **7**, 12054.

7 B. Sentürk, B. Butschke and F. Eisenreich, *Chem. Sci.*, 2025, **16**, 3130–3140.

8 J. Copko and T. Slanina, *Chem. Commun.*, 2024, **60**, 3774–3777.

9 F. M. Raymo and M. Tomasulo, *J. Phys. Chem. A*, 2005, **109**, 7343–7352.

10 N. Huang, N. Zhao, C. Zhang, C. Li, X. Wei, Y. Zhang, Y. Bao and S. Wang, *ACS Appl. Nano Mater.*, 2023, **6**, 15302–15313.

11 R. Guo, K. Hu, P. He, Y. Ni, K. Liu, H. Wu, L. Huang and L. Chen, *Appl. Phys. A*, 2020, **126**, 812.

12 M. Mostaghimi, H. P. Hernandez, Y. Jiang, W. Wenzel, L. Heinke and M. Kozlowska, *Commun. Chem.*, 2023, **6**, 275.

13 A. V. Mumyatov, L. A. Frolova, L. G. Gutsev, E. A. Khakina, N. A. Sanina, S. M. Aldoshin and P. A. Troshin, *J. Mater. Chem. C*, 2023, **11**, 963–969.

14 Z. Li, X. Zeng, C. Gao, J. Song, F. He, T. He, H. Guo and J. Yin, *Coord. Chem. Rev.*, 2023, **497**, 215451.

15 J. Zhu, X.-W. Sun, X. Yang, S.-N. Yu, L. Liang, Y.-Z. Chen, X. Zheng, M. Yu, L. Yan, J. Tang, W. Zhao, X.-J. Yang and B. Wu, *Angew. Chem., Int. Ed.*, 2023, **62**, e202314510.

16 J. Wang, L. Avram, Y. Diskin-Posner, M. J. Białek, W. Stawski, M. Feller and R. Klajn, *J. Am. Chem. Soc.*, 2022, **144**, 21244–21254.

17 C. Zeng, H. Rajput, J. R. Brown, B. Liu, T. E. Long and P. Westerhoff, *ACS Appl. Polym. Mater.*, 2024, **6**, 362–370.

18 A. R. Sekhar, Y. Chitose, J. Janoš, S. I. Dangoor, A. Ramundo, R. Satchi-Fainaro, P. Slavíček, P. Klán and R. Weinstain, *Nat. Commun.*, 2022, **13**, 3614.

19 L. J. G. W. van Wilderen, D. Kern-Michler, C. Neumann, M. Reinfelds, J. von Cosel, M. Horz, I. Burghardt, A. Heckel and J. Bredenbeck, *Chem. Sci.*, 2023, **14**, 2624–2630.

20 S. Mondal, W. L. Koay, I. Daga, S. Paul, V. X. Truong and N. D. P. Singh, *J. Am. Chem. Soc.*, 2024, **146**, 23376–23386.

21 M. Sack, K. Hölz, A.-K. Holik, N. Kretschy, V. Somoza, K.-P. Stengele and M. M. Somoza, *J. Nanobiotechnol.*, 2016, **14**, 14.

22 S. Leichnitz, K. C. Dissanayake, A. H. Winter and P. H. Seeberger, *Chem. Commun.*, 2022, **58**, 10556–10559.

23 X.-J. Tang, Y. Wu, R. Zhao, X. Kou, Z. Dong, W. Zhou, Z. Zhang, W. Tan and X. Fang, *Angew. Chem., Int. Ed.*, 2020, **59**, 18386–18389.

24 H. Guo, Z. Zhang, Y. Chen, H. Yang, L. Deng, J. Dai, M. Cong, B. Wang, D.-H. Qu, W.-H. Zhu, J. Zhang and H. Tian, *Angew. Chem., Int. Ed.*, 2025, **64**, e202425313.

25 T. Liu, B. Bao, Y. Li, Q. Lin and L. Zhu, *Prog. Polym. Sci.*, 2023, **146**, 101741.

26 L. T. B. Nguyen and M. Abe, *Bull. Chem. Soc. Jpn.*, 2024, **97**, uoae067.

27 T. Saßmannshausen, A. Kunz, N. Oberhof, F. Schneider, C. Slavov, A. Dreuw, J. Wachtveitl and H. A. Wegner, *Angew. Chem., Int. Ed.*, 2024, **63**, e202314112.

28 T. Wu, H. Tang, C. Bohne and N. R. Branda, *Angew. Chem., Int. Ed.*, 2012, **51**, 2741–2744.

29 Q.-q. Tan, Y. Guo, D. L. Phillips, T. Xu and J. Ma, *J. Phys. Chem. Lett.*, 2023, **14**, 2119–2124.

30 Y. Guo, M. Dai, D. L. Phillips, W. Xu and J. Ma, *J. Phys. Chem. Lett.*, 2022, **13**, 3417–3423.

31 Y. Su, D. Zheng, L. Ge, L. Yu, D. Lee Phillips, J. Ma and Y. Fang, *Chem. Sci.*, 2024, **15**, 20556–20564.

32 O. Galangau, S. Delbaere, N. Ratel-Ramond, G. Rapenne, R. Li, J. P. D. C. Calupitan, T. Nakashima and T. Kawai, *J. Org. Chem.*, 2016, **81**, 11282–11290.

33 A. V. Zakharov, A. V. Yadykov, E. B. Gaeva, A. V. Metelitsa and V. Z. Shirinian, *J. Org. Chem.*, 2021, **86**, 16806–16814.

34 T. Nakashima, K. Tsuchie, R. Kanazawa, R. Li, S. Iijima, O. Galangau, H. Nakagawa, K. Mutoh, Y. Kobayashi, J. Abe and T. Kawai, *J. Am. Chem. Soc.*, 2015, **137**, 7023–7026.

35 R. Li, T. Nakashima and T. Kawai, *Chem. Commun.*, 2017, **53**, 4339–4341.

36 C. J. Martin, M. Minamide, J. P. D. C. Calupitan, R. Asato, J. Kuno, T. Nakashima, G. Rapenne and T. Kawai, *J. Org. Chem.*, 2018, **83**, 13700–13706.

37 C. L. Fleming, S. Li, M. Grøtli and J. Andréasson, *J. Am. Chem. Soc.*, 2018, **140**, 14069–14072.

38 X. Li, Z. Lin, Y. Tian, C. Zhang, P. Zhang, R. Zeng, L. Qiao and J. Chen, *Anal. Bioanal. Chem.*, 2023, **415**, 715–724.

39 T. Asano and T. Okada, *J. Org. Chem.*, 1984, **49**, 4387–4391.

40 R. Weinstain, T. Slanina, D. Kand and P. Klán, *Chem. Rev.*, 2020, **120**, 13135–13272.

41 M. J. Frisch, G. W. Trucks, H. B. Schlegel, G. E. Scuseria, M. A. Robb, J. R. Cheeseman, G. Scalmani, V. Barone, G. A. Petersson, H. Nakatsuji, X. Li, M. Caricato, A. V. Marenich, J. Bloino, B. G. Janesko, R. Gomperts, B. Mennucci, H. P. Hratchian, J. V. Ortiz, A. F. Izmaylov, J. L. Sonnenberg, D. Williams-Young, F. Ding, F. Lipparini, F. Egidi, J. Goings, B. Peng, A. Petrone, T. Henderson, D. Ranasinghe, V. G. Zakrzewski, J. Gao, N. Rega, G. Zheng, W. Liang, M. Hada, M. Ehara, K. Toyota, R. Fukuda, J. Hasegawa, M. Ishida, T. Nakajima, Y. Honda, O. Kitao, H. Nakai, T. Vreven, K. Throssell, J. A. Montgomery Jr., J. E. Peralta, F. Ogliaro, M. J. Bearpark, J. J. Heyd, E. N. Brothers, K. N. Kudin, V. N. Staroverov, T. A. Keith, R. Kobayashi, J. Normand, K. Raghavachari, A. P. Rendell, J. C. Burant, S. S. Iyengar, J. Tomasi, M. Cossi, J. M. Millam, M. Klene, C. Adamo, R. Cammi, J. W. Ochterski, R. L. Martin, K. Morokuma, O. Farkas, J. B. Foresman and D. J. Fox, *Gaussian 16*, 2016.